

Article

Chemical Treatment of Banana Blossom Peels Adsorbent as New Approach for Manganese Removal: Isotherm and Kinetic Studies

Nurul Nadia Rudi ¹, Najeeha Mohd Apandi ^{2,*} , Mimi Suliza Muhamad ^{3,*} , Norshuhaila Mohamed Sunar ^{4,*},
Affah Mohd Apandi ⁵ , Lee Te Chuan ⁶, Ramathanan Nagarajah ² and Suhair Omar ²

¹ KH Tekjaya Sdn. Bhd. 46, Jalan Servis, Georgetown 10050, Malaysia; nurulnadiarudi@gmail.com

² Department of Civil Engineering Technology, Faculty of Civil Engineering Technology, Universiti Tun Hussein Onn Malaysia, Pagoh Education Hub, Pagoh, Muar 84600, Malaysia

³ Sustainable Engineering Technology Research Centre (SETechRC), Faculty of Engineering Technology, Universiti Tun Hussein Onn Malaysia, Pagoh Education Hub, Pagoh, Muar 84600, Malaysia

⁴ Research Centre for Soft Soil (RECESS), Universiti Tun Hussein Onn Malaysia, Parit Raja, Batu Pahat 86400, Malaysia

⁵ Department of English Language and Linguistics, Centre for Language Studies, Universiti Tun Hussein Onn Malaysia, Parit Raja, Batu Pahat 86400, Malaysia; affah@uthm.edu.my

⁶ Department of Production and Operation Management, Faculty of Technology Management and Business, Universiti Tun Hussein Onn Malaysia, Parit Raja, Batu Pahat 86400, Malaysia; tlee@uthm.edu.my

* Correspondence: najeeha84@gmail.com (N.M.A.); msuliza@uthm.edu.my (M.S.M.); shuhaila@uthm.edu.my (N.M.S.)

Abstract: This research aimed to investigate the potential of chemically modified banana blossom peels (BBP) as an adsorbent for removing manganese (Mn) from water. Zeta potential, field emission scanning electron microscopy (FESEM), Fourier transform infrared spectroscopy (FTIR), X-ray diffraction (XRD), and Brunauer–Emmet–Teller (BET) were used to characterise the BBP adsorbent. Batch adsorption studies were used to assess the effects of the solution pH, adsorbent dosage, initial manganese concentration, and contact time of the adsorption process. Zeta potential of BBP with a value of -9.87 to -21.1 mV and FESEM analysis revealed deeper dents and rough internal surfaces conducive to Mn deposition, whereas EDX analysis revealed the presence of C, O, and Na elements (before adsorption); C, O, and Mn (after adsorption). The presence of hydroxyl, carboxylic, and amino groups, which are responsible for the adsorption process, was discovered using FTIR analysis. Furthermore, XRD analysis revealed that the BBP adsorbent structure is amorphous. The BBP adsorbent has a BET surface area of 2.12 m²/g, a total pore volume of 0.0139 cm³/g, and an average pore diameter of 64.35 nm. The BBP adsorbent demonstrated remarkable results of 98% Mn removal under the optimum pH 7, 0.5 g (adsorbent dosage), and 10 mg/L of Mn initial concentration in 150 min of contact time. The linear Langmuir and Freundlich isotherm models best fit the adsorption isotherm data with the $R^2 > 0.98$. In contrast, the adsorption process occurs as a function of the chemisorption as determined by linear pseudo-second-order kinetics. Using 0.1 M HCl, the maximal desorption rate of Mn was 92% in the first cycle, with a recovery rate of 94.18% Mn removal in 30 min. These findings support the use of BBP as a natural adsorbent for Mn removal as a treatment option for improving wastewater quality.

Keywords: banana blossom peels; manganese; adsorption isotherm; kinetic study; desorption



Citation: Rudi, N.N.; Mohd Apandi, N.; Muhamad, M.S.; Mohamed Sunar, N.; Mohd Apandi, A.; Te Chuan, L.; Nagarajah, R.; Omar, S. Chemical Treatment of Banana Blossom Peels Adsorbent as New Approach for Manganese Removal: Isotherm and Kinetic Studies. *Sustainability* **2023**, *15*, 10223. <https://doi.org/10.3390/su151310223>

Academic Editors: Ahmed Osman, Oh Wen Da and Pow Seng Yap

Received: 29 March 2023

Revised: 6 June 2023

Accepted: 15 June 2023

Published: 28 June 2023



Copyright: © 2023 by the authors. Licensee MDPI, Basel, Switzerland. This article is an open access article distributed under the terms and conditions of the Creative Commons Attribution (CC BY) license (<https://creativecommons.org/licenses/by/4.0/>).

1. Introduction

Water pollution has increased due to rapid industrial development [1]. The annual disposal of contaminants such as toxic sludge, solvents, and heavy metals into water bodies has been estimated to be between 300 and 400 million tonnes [2]. Due to unregulated waste disposal and effluent discharge from industry, Malaysia's number of polluted water sources grows over time [3]. The presence of heavy metals such as manganese (Mn) identified in

rivers due to discharge from industrial effluents had alarmed the waterworks company [4]. Mn was frequently employed in steel manufacture and was emitted in industrial effluents. It is a trace element in various minerals, including oxides, carbonates, and silicates, with pyrolusite (manganese dioxide) being the most prevalent naturally occurring form [5]. Mn may be found in many oxidation states and species in the earth's crust and water sources [6]. When Mn is oxidised, it becomes insoluble in water and alters the colour of the water to a brownish-red colour, rendering it aesthetically unappealing and unsafe for drinking [3,7–9]. Consumption of that high Mn concentration in drinking water has been linked to neurological abnormalities and adverse effects on intellectual development and cognitive development [9,10].

An excessive Mn ion accumulation in specific brain locations can result in neurotoxicity and degenerative brain disease [11]. Children exposed to 240–350 µg/L Mn ions showed indications of decreased manual agility, speed, short-term memory, and visual recognition [12]. Manganese-containing water has been treated using chemical precipitation, ultraviolet irradiation, membrane filtration, ozone, ion exchange, oxidation, and electrochemical treatment [13–21]. Various treatment technologies can remove Mn in water; however, some problems arise, such as complex processes, space requirements, treatment capacity, sludge disposal, and high operational and maintenance costs [3,8,22]. The adsorption process is one of the potential alternatives for low-cost and efficient methods to improve surface water quality [23,24]. This process has been broadly studied to develop high selectivity and efficient adsorbent materials [25–27]. The materials for adsorbents are relatively cheap, less toxic, easy to be functionalised over other substrates, and highly efficient.

Agricultural waste adsorbent mainly has gained attention among researchers in treating water containing Mn ions owing to its efficiency and availability and because it is environmentally friendly and easy to produce [22,28]. The adsorption process has effectively removed contaminants with minimal problems among the treatment technologies. Agricultural waste from banana trees is found abundantly in Malaysia and can be utilised to produce low-cost adsorbents. Banana trees are widely cultivated and used for a variety of purposes. Bananas account for about 16% of overall fruit output, making them the second-largest fruit globally, with Malaysia accounting for 32% of total fruit production [29]. Research on the banana blossom as an adsorbent for contaminant removal is limited. The banana blossom peels (BBP) adsorbent can remove 79.72% turbidity, 88.24% total solids, and 61.01% chloride from a lake water sample while also lowering the water's alkalinity to neutral pH. (8.4 to 6.75). However, the composition of BBP can vary depending on the maturity of the plant and other factors. Nevertheless, the chemical treatment of BBP as an adsorbent for Mn removal has not been investigated before.

No research has been done on the isotherm and kinetic studies of the chemically modified BBP adsorbent's reusability and use for Mn removal. Therefore, the current study attempts to synthesise banana blossom peels using a chemical treatment method. The effects of several process variables, such as adsorbent dose, contact time, pH, and initial manganese concentration, on the adsorption behaviour of Mn onto the BBP adsorbent were examined. Isotherm and kinetic studies were used to figure out how the adsorption process works.

2. Materials and Methods

2.1. Banana Blossom Peels Adsorbent Preparation

Banana blossom peels (BBP) were collected from banana planters at Pagoh Jaya, Muar, Johor, Malaysia. The BBP was properly scrubbed and washed to eliminate surface contaminants; the BBP was then chopped into tiny pieces and oven-dried for 12 h at $60\text{ }^{\circ}\text{C} \pm 1\text{ }^{\circ}\text{C}$. The BBP was grounded and sieved into powder with a standard mesh ring of 150–212 µm. The BBP powder was submerged in 20 mL of 1 M HCl and sodium hydroxide (NaOH). The alkaline–acid treatment has demonstrated potential as a cost-effective method for modifying adsorbents, leading to their enhance efficiency for water treatment [30]. The BBP powder was mixed for 30 min with chemical activation solutions in an orbital shaker

at 150 rpm. Any remaining chemicals on the surface were removed by rinsing the BBP with distilled water. The BBP powder was then dried for 12 h at $60\text{ }^{\circ}\text{C} \pm 1\text{ }^{\circ}\text{C}$ for 12 h [31] and sieved using a standard 60 mesh sieve. Figure 1 shows a schematic illustration of BBP adsorbent preparation.

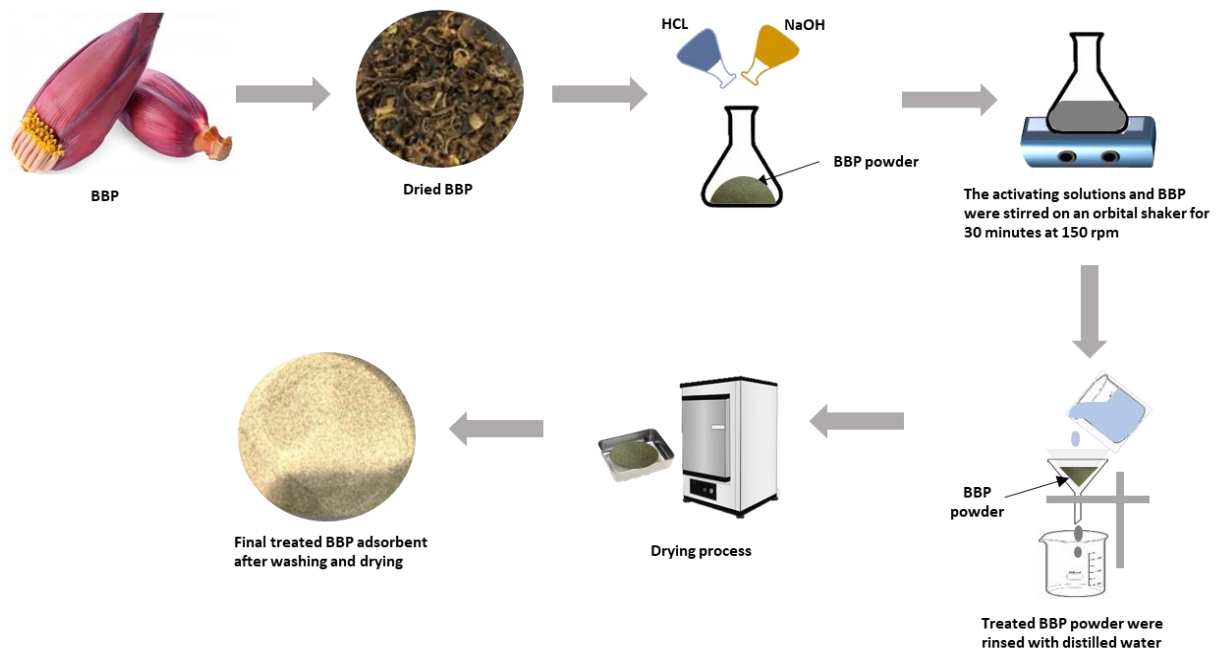


Figure 1. Schematic illustration of BBP adsorbent preparation using chemical treatment.

2.2. Characterisation of Banana Blossom Peels Powder

The elemental content and surface morphology of the BBP adsorbent were defined using field emission scanning electron microscope (FESEM) and energy dispersive X-ray (EDX). Fourier transform infrared spectroscopy (FTIR) was used to look at the functional groups in the BPP adsorbent. The FTIR spectrum was performed with a resolution of 4 cm^{-1} , and the reading was taken in the mid-infrared range of $4000\text{ to }400\text{ cm}^{-1}$. The crystalline structure of the BBP pattern was determined using an X-ray diffraction (XRD) pattern created by Cu K α monochromatic radiation utilising Bruker D8 Advanced X-rays of 1.5406 \AA wavelength. The BBP adsorbent was compressed in a cassette sample holder and the data were collected from $2\theta = 20^{\circ}\text{--}80^{\circ}$ with a sampling pitch of 0.02° . Based on nitrogen adsorption–desorption at 77 K (Thermo Scientific surface area and pore analyser), a Brunauer–Emmet–Teller (BET) method was used to measure the surface area, total pore volume, and pore diameter. The BBP adsorbent sample was outgassed at $60\text{ }^{\circ}\text{C}$ for 24 h prior to analysis.

Zeta Potential

The charge of zeta potential of the BBP adsorbent was determined by measuring their velocity by Zetasizer Nano Series ZSP system (Malvern Instruments, Worcestershire, UK). Additionally, the zeta potential of the BBP adsorbent was measured at the pH value in the vitro digestion model according to Anai Zavala-Franco et al. [32].

2.3. Batch Adsorption Experiment

Stuart orbital shaker was used for batch adsorption experiments where a 250 mL conical flask was shaken at 150 rpm with initial Mn^{2+} concentrations (10–50 mg/L), adsorbent dosage (0.1–0.7 g/L), varied pH (4–9), and contact time (60–80 min). By dissolving 0.308 g manganese (II) sulphate in 1 L deionised water, a stock solution containing 100 mg/L Mn was obtained. The experimental solutions were diluted further in 1 L flasks to concentra-

tions ranging from 10 to 50 mg/L. The following equations were used to determine the effectiveness of Mn removal (%) and adsorption capacity, q_e (mg/g):

$$\text{Removal}(\%) = \frac{(C_o - C_e)}{C_o} \times 100 \quad (1)$$

$$q_e = \frac{V(C_o - C_e)}{W} \quad (2)$$

where

C_o (mg/L): Initial Mn concentration

C_e (mg/L): Equilibrium Mn concentration in solution

q_e (mg/g): The amount of metal ions

V: The solution volume (L)

W: The mass of the BBP adsorbent (g)

The sample's suspension was filtered with 0.45 μm filter paper before being analysed for Mn concentration using inductively coupled plasma optical emission spectrometry (ICP-OES) (Optima 800, Perkin Elmer, Waltham, MA, USA). The concentration of Mn was determined using this approach before and after the batch adsorption tests.

2.4. Adsorption Isotherms Studies

In the liquid state, adsorption isotherms are useful for demonstrating the behaviour, mechanism, and optimal fit of metal ion concentration on the surface of adsorbents at a certain concentration [33,34]. This study employed the Langmuir and Freundlich models in order to study the link between the Mn concentration adsorbed by BPP and the linear and non-linear equations. Solute monolayer adsorption onto an adsorbent surface was considered to represent the Langmuir isotherm, and the equation is as follows:

Linear:

$$\frac{C_e}{q_e} = \frac{1}{q_{max}b} + \frac{C_e}{q_{max}} \quad (3)$$

Non-Linear:

$$q_e = \frac{q_{max} \pm bC_e}{(1 + bC_e)} \quad (4)$$

C_e is the solute equilibrium concentration, q_{max} is the adsorbent monolayer capacity (mg/g), and b is the adsorption constant (L/mg). C_e/q_e versus C_e should be plotted as a straight line [35].

Non-ideal, reversible adsorption is commonly described by the Freundlich isotherm. The equation is as follows:

Linear:

$$\log q_e = \log K_f + \frac{1}{n} \log C_e \quad (5)$$

Non-Linear:

$$q_e = K_f + C_e^{1/n} \quad (6)$$

q_e is the absorption of pollutant per unit weight of biosorption (mg/L), and K_f is the Freundlich constant defining the adsorption capacity (mg/L). C_e is the equilibrium concentration (mg/L), and n denotes the adsorption intensity empirical constant.

2.5. Adsorption Kinetics Studies

The Mn removal data from the experiment under ideal circumstances were used for linear and non-linear models of pseudo-first-order and second-order kinetics to create the prediction adsorption data. The kinetic study may be utilised to determine the adsorption process's reaction rate and mechanism. Adsorption rates of Mn ions are assumed to be inversely related to the number of empty spaces on the BBP adsorbent.

The pseudo-first-order equation for adsorption of a solute from a liquid solution is as follows:

Linear:

$$\ln(q_e - q_t) = \ln q_e - K_1 t \quad (7)$$

Non-Linear:

$$q_t = q_e (1 - e^{-K_1 t}) \quad (8)$$

q_e is the adsorbed metal ion mass at equilibrium (mg/g), q_t is the adsorbed metal ion mass at time t (mg/g), and K_1 is the pseudo-first-order reaction rate constant (1/min). Meanwhile, the pseudo-second-order kinetic model proposes that chemical adsorption that incorporates valence forces through electron sharing or exchange between adsorbent and adsorbate might be the rate-limiting step [34,36].

The adsorption equilibrium capacity determines the pseudo-second-order equation, as illustrated below:

Linear:

$$\frac{t}{q_t} = \frac{1}{K_2 q_e^2} + \frac{t}{q_e}$$

Non-Linear:

$$q_t = \frac{k^2 q_e^2 t}{1 + k^2 q_e t}$$

The pseudo-second-order reaction rate equilibrium (g/mg min) is represented by the constant K_2 .

2.6. Desorption Experiment

The desorption experiment was conducted to test the BBP adsorbent's reusability. In a conical flask, 100 mL of 0.5 M HCL was contacted with manganese pre-sorbed BBP adsorbent samples (0.5 g) and shaken at 150 rpm at room temperature. After that, the sample was taken at regular intervals and filtered before being analysed for manganese levels using ICP-OES.

3. Results and Discussion

3.1. Characterisation of BBP Adsorbent

3.1.1. Zeta Potential

The electrokinetic potential in colloidal systems is known as zeta potential; it can also describe the surface of charged particles. The zeta potential can be influenced by both surface charge and ambient factors, and it may be affected by pH and ions in the medium as a result. In the present study, a zeta potential value of -9.87 to -21.1 mV (Figure 2) was obtained in the BBP adsorbent. These results are in slight accordance with Anai Zavala-Franco et al. [32], who reported BBP zeta potential values of -12.7 to -14 mV, respectively. High zeta potential indicates strongly charged particles, which precludes particle aggregation owing to electrostatic repulsion. The attraction will overpower the repulsion if the zeta potential value is low and it is prone to form coagulates [37].

3.1.2. Surface Morphology and EDX Analysis

Figure 3 shows the surface morphology, microstructures, and physical characteristics of the BBP adsorbent before and after Mn adsorption, respectively, as measured by FESEM. The BBP adsorbent's surface is crimped with deeper dents, has a rough interior surface, and is dense (Figure 2). Due to extremely uneven surfaces that give maximal surface area for manganese ion adsorption, the shape of BBP may enhance Mn adsorption [35,37–39]. EDX examination revealed the presence of significant carbon (C), oxygen (O), and sodium (Na) components in Figure 3a,b.

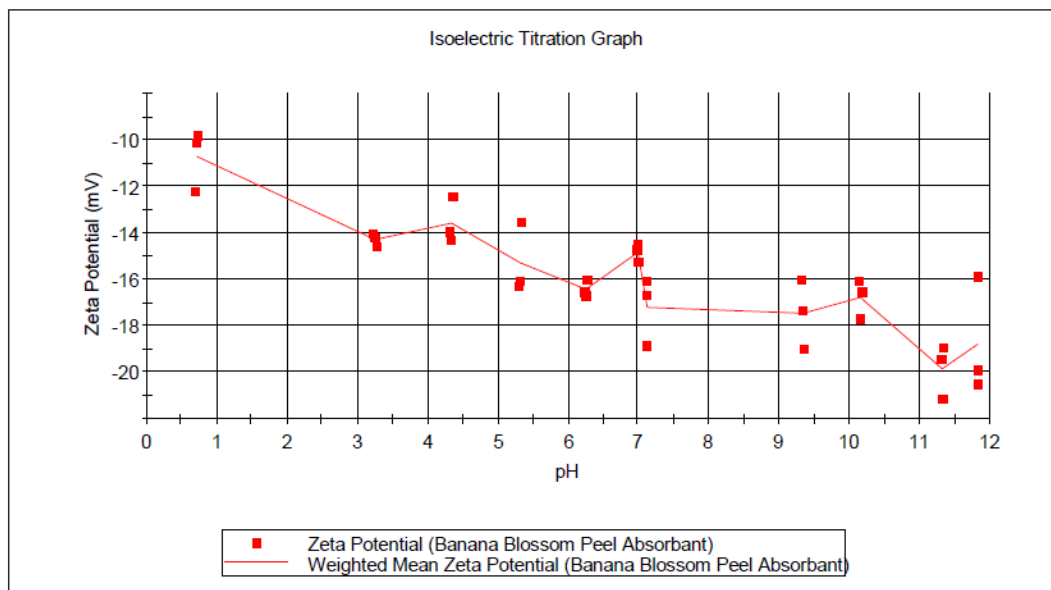


Figure 2. Zeta potential of banana blossom peel adsorbent.

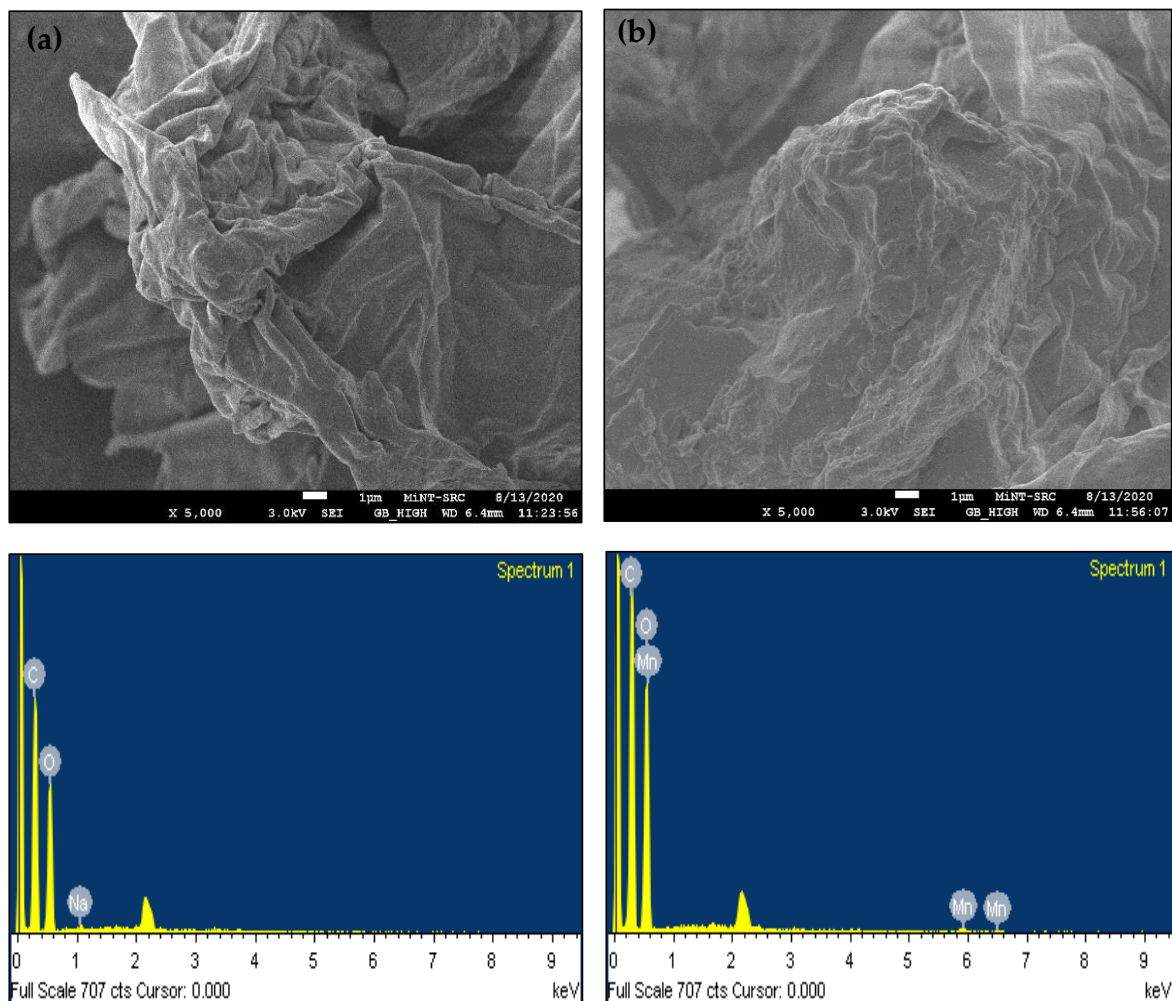


Figure 3. Scanning electron microscopic images of pristine BBP adsorbent (a) before and (b) after adsorption of Mn with EDX analysis.

The FESEM micrograph is used to visualize the surface morphology of the BBP adsorbent and shows changes in form, suggesting Mn adsorption onto the BBP. Figure 3b shows how the morphologies of FESEM modify the adsorption process with a less crimped and rough surface than the new BBP adsorbent. Because of the intense shaking and interactions with the Mn solutions and water molecules, the surfaces became loose and porous, forming micro-channels by Mn ion penetration into the interior binding sites [39]. Following the adsorption, gleaming particles were discovered on the surface of the BBP. In addition, the EDX spectra in Figure 4 show an additional Mn signal, indicating that Mn ions have been uptaken onto the surface of the BBP adsorbent.

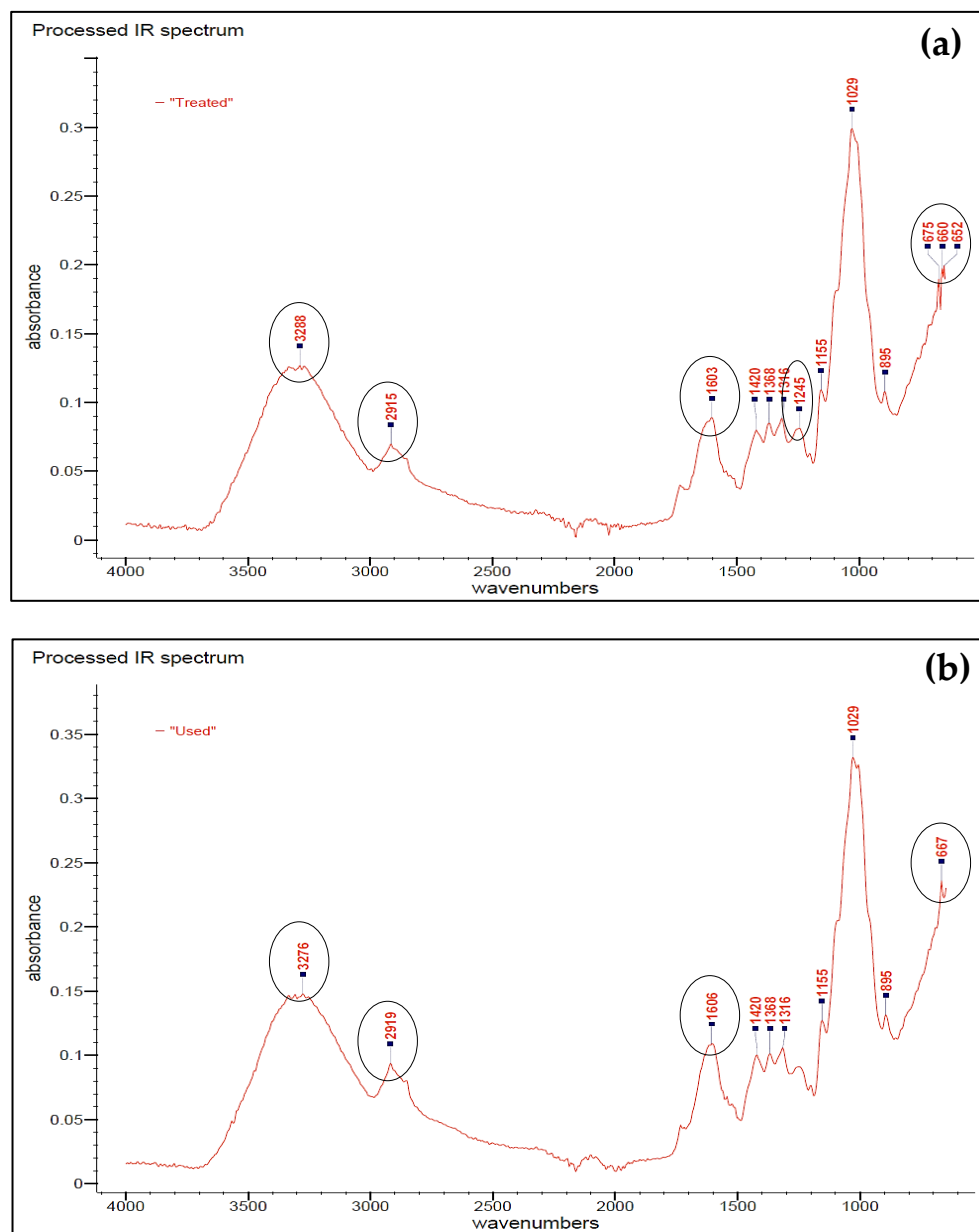


Figure 4. FTIR analysis of BBP adsorbent (a) before and (b) after manganese adsorption processes of Mn.

3.1.3. FTIR Analysis

Figure 4a,b illustrates the functional groups found in the BBP adsorbent before and after manganese adsorption, respectively. The broad transmission band at roughly 3288 cm^{-1} can be attributed to the overlapping of hydroxyl group O-H (carboxylic acid), C-O stretching, and N-H (amino groups) of macromolecular association [33], as seen in Figure 4a.

Figure 4b shows that the -OH or -NH stretch band was displaced to 3276 cm^{-1} , indicating that the adsorption involves -OH and C-O stretching of alcohol or -NH deformation [40]. In Figure 4a, BBP has a C-H stretching vibration of 2915 cm^{-1} , which shifts to 2919 cm^{-1} in Figure 4b, indicating the existence of an alkene functional group [8,41].

The asymmetric stretching of the carboxylic C=O double bond, which is prevalent in pectin-containing fibre materials, correlates to changes in the band from 1603 cm^{-1} (Figure 4a) to 1606 cm^{-1} (Figure 4b). The peaks at 1245 cm^{-1} are created by C-O stretching vibrations in hemicellulose and C-O stretching vibrations in the acetyl group in lignin, as shown in Figure 4a. The absence of the 1245 cm^{-1} peak noticed in Figure 5b after the adsorption process pointed to the loss of hemicellulose and lignin [42]. The change of bands observed from $675\text{--}652\text{ cm}^{-1}$ in Figure 4a to a single band of 667 cm^{-1} , in Figure 4b, may represent the aromatic C-H groups [43]. The presence of functional groups (hydroxyl, carboxyl, amine, etc.) in the BBP adsorbent had contributed to the adsorption.

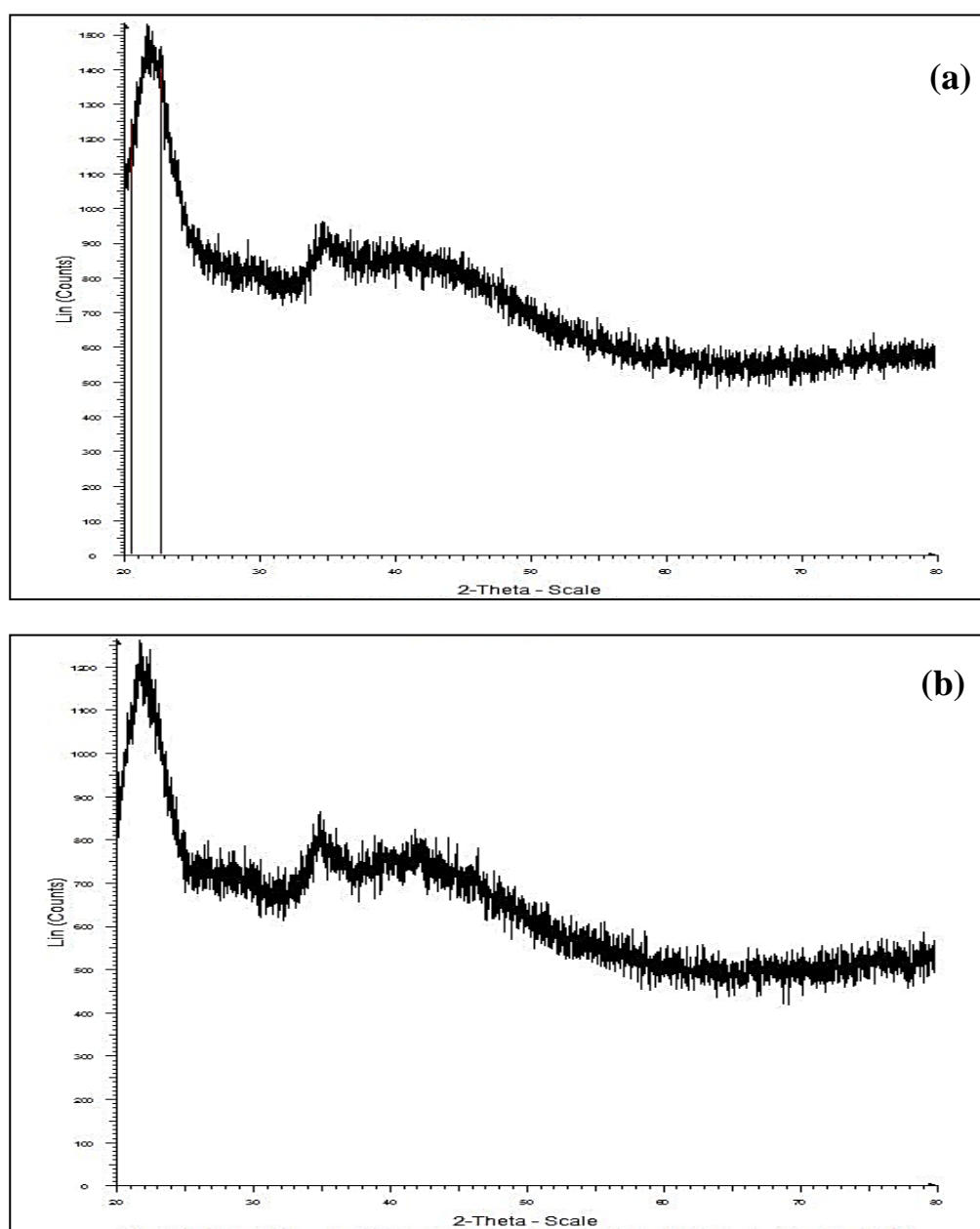


Figure 5. XRD pattern of BBP adsorbent (a) before and (b) after manganese adsorption.

3.1.4. XRD Analysis

Figure 5a,b shows XRD analysis of the BBP adsorbent before and after manganese adsorption, respectively. The absence of sharp peaks and the appearance of a broad low-intensity diffraction background indicate that the structure of the BBP adsorbent is an amorphous phase connected to the carbon structure [39]. Other than that, it is also due to organic materials and volatile substances. The existence of typical crystalline cellulose peaks was discovered at a temperature of $2\theta \approx 22^\circ$. The crystal structure of cellulose [44] is thought to be responsible for the peak. There were no significant variations in the crystalline peaks of the BBP adsorbent after adsorption, except that the intensity of the phases decreased, indicating that manganese ions were replacing the ions and changing the structure of the BBP adsorbent. This reveals that manganese adsorption did not alter the structural space of BBP adsorbents, and, hence, the adsorption process happened on the surface.

3.1.5. BET Analysis

Adsorption is a complicated process influenced by several parameters, including the adsorbent's pore structure, size, and surface chemistry. The interpretation of Figure 6; the red line (represents the adsorption isotherm) and blue dot (represents the isotherm corresponds to the point of maximum inflection known as the monolayer coverage point). The average pore diameter of the BBP adsorbent is 64.35 nm, with a BET surface area of $2.12 \text{ m}^2/\text{g}$, and a total pore volume of $0.0139 \text{ cm}^3/\text{g}$. Figure 6 shows the nitrogen adsorption–desorption isotherms and pore size distribution curves (inset) of the BBP adsorbent. According to the IUPAC classification, the isotherm for the BBP adsorbent is classed as type 3 macropores ($>50 \text{ nm}$). Because it has an ionic radius of roughly 0.80 nm , the pore size distribution makes it excellent for adsorbing manganese ions [45]. Manganese ions were, therefore, able to enter the biggest micropores (less than 2 nm , according to IUPAC classification). Most agro- or carbonaceous materials have a low surface area [31], but a material's low surface area does not imply a low adsorption capacity [46]. The functional groups (amino, carbonyl, carboxyl) present in the structure of the adsorbent are primarily responsible for the adsorption capabilities of non-living biomasses [47].

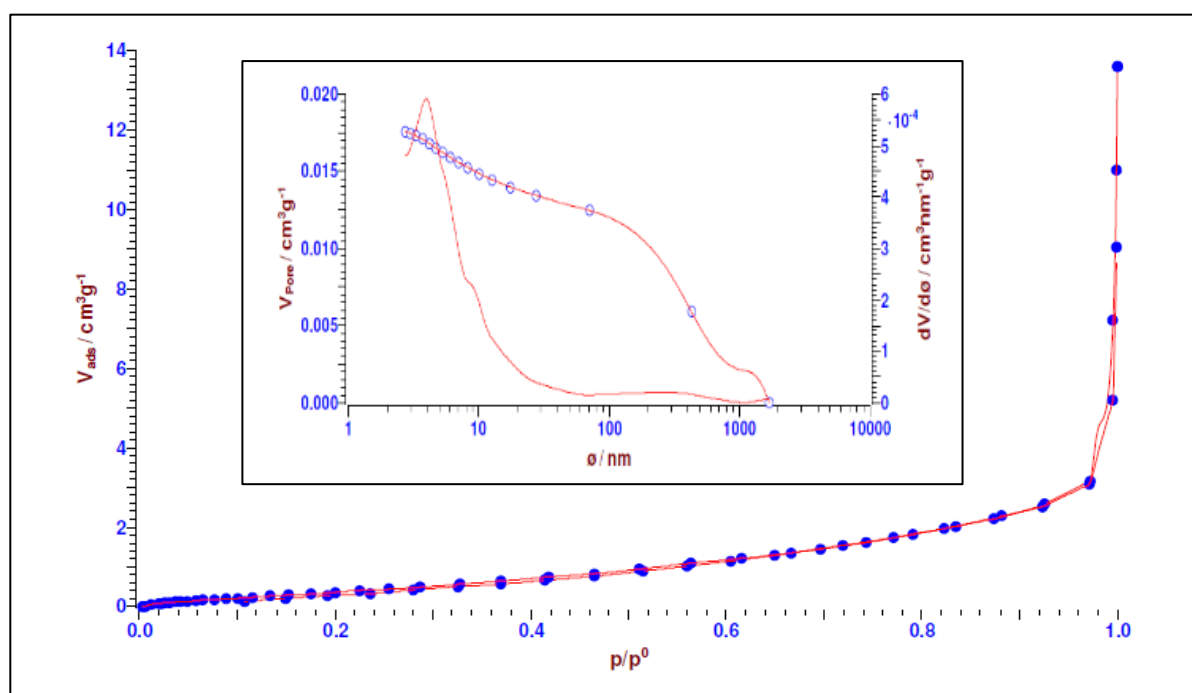


Figure 6. Nitrogen adsorption–desorption isotherms and pore size distribution curves (inset) of BBP adsorbent.

3.2. Batch Adsorption Studies

3.2.1. Effect of pH

Figure 7 displays the optimal performance of various pH conditions with a 0.1–0.7 g adsorbent dosage and initial manganese concentrations ranging from 10–50 mg/L in 60–180 min of contact time. The effect of pH ranges from 5–9 on the removal of Mn by the BBP adsorbent, as is shown in Figure 7a. The impact of pH may be explained using the surface charge on the BBP adsorbent. The elimination of Mn was shown to be at a maximum of 90% at pH 7 when the initial pH was elevated but then gradually reduced over 7. The adsorption increased when the pH of the solution increased because more negative-charged, metal-binding sites were exposed, attracting positive-charged metal ions and inducing adsorption onto the adsorbent surface [48]. The positive charge density of the H^+ ion decreases with increasing pH, which reduces electrostatic repulsion on the surface of the BBP adsorbent and attracts more manganese ions, thus facilitating greater metal adsorption [35]. The lowest percentage removal of Mn^{2+} was found at pH 4 and pH 5.5. This is due to the fact that the substantial H^+ ion concentration adsorbs most of the adsorbent's active site at low pH, which lowers manganese ion removal efficacy [41].

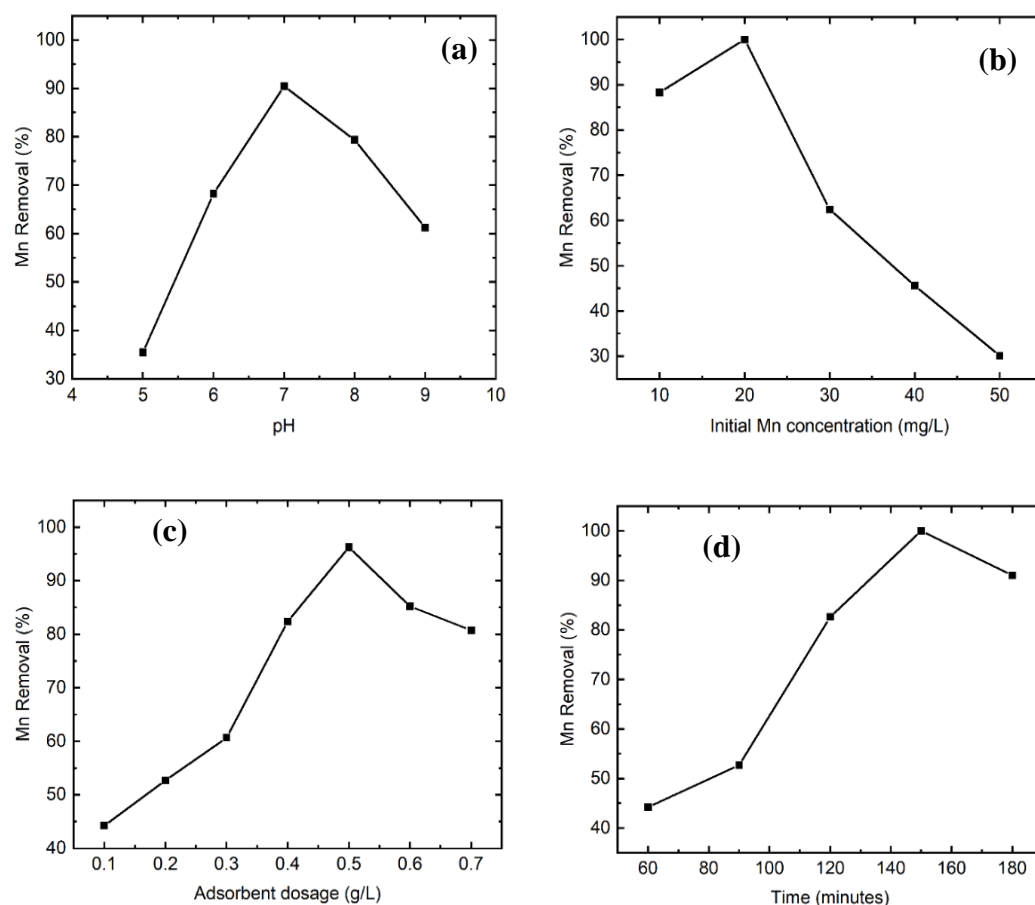


Figure 7. Effect of (a) pH, (b) initial Mn concentration (mg/L), (c) BBP adsorbent dosage (g/L), and (d) contact time (minutes) for Mn removal.

Saturation of the bonded active sites took place and became inaccessible to other cations [38]. The surface charge on solid particles is highly affected by pH solution [49]. The chemical state of the functional groups and the properties and availability of metal ions in the solution are also altered by the absorption process [41]. When pH rises, partial hydrolysis of Mn^{2+} ions occurs, resulting in the formation of OH^- complexes such as $Mn(OH)^+$, $Mn(OH)_2$, $Mn_2(OH)^{3+}$, and Mn_2OH^{3+} in solution. As a result, adsorption and precipitation of manganese–hydroxyl compounds inside the adsorbent structure may be

involved [50]. The surface functional groups of the BBP adsorbent and the metal chemistry in the solution are linked to Mn adsorption at higher pH. The functional groups may be observed in the preceding section, in Figure 5. Feizi and Jalali [51] stated that metal sorption is dependent on the dissociation of carboxyl and hydroxyl groups. The functional groups would be exposed when the pH increased. As a result, increasing the density of negative charge on the BBP adsorbent's surface aids in the attraction of manganese ions to functional groups [38]. The pH value, as well as surface charge and ionisation, are used to determine the adsorption capacity of the BBP adsorbent. Therefore, pH 7 is the optimum pH value for maximum Mn removal in the present study.

3.2.2. Effect of Initial Manganese Concentration

Figure 7b shows the effect of the initial Mn ion concentration of 10–50 mg/L when the BBP adsorbent solution was used with the ideal pH of 8, as stated in the previous section. The proportion of Mn removed was expected to decrease as the initial Mn ion concentration increased. The overall Mn removal was 100% at a starting Mn value of 20 mg/L. A trend was observed in Figure 8b, where Mn removal was decreased from 100% to 32%, with an increased initial Mn concentration from 10–50 mg/L. This means that the surface saturation is influenced by the manganese content at the start. At greater manganese concentrations, the adsorbent surface area saturates as ion transport from the bulk solution to the adsorbent surface area decreases [8]. Idrees et al. [52] suggested that the initial concentration of manganese ions in the adsorbent and solution provides an impelling reason to overcome metal transfer resistances in the adsorbent and solution. As a result, the active sites of the BBP adsorbent and manganese ions collide with a higher probability. At some point, the adsorption sites become occupied and achieve a fixed value, making further adsorption from an aqueous solution impossible. Adeogun et al. [53] also found that when the initial Mn concentration increased, the removal of Mn ions using raw and oxalic acid-modified rice husk adsorbent reduced. Adsorption happens quickly on the exterior surface of the adsorbent, followed by a delayed interior diffusion phase, which may be the rate-determining step. This is similar to this study, in which the rate of adsorption is fast for the first 10 min, then slows until virtual equilibrium is reached due to the rapid occupancy of Mn ions onto the surface of the BBP adsorbent.

3.2.3. Effect of Adsorbent Dosage

Figure 7c shows the impact of BBP dose on manganese removal at pH 7 with an ideal beginning Mn content of 20 mg/L. Adsorbent dosages ranging from 0.1 g/L to 0.7 g/L were used, and the tests were shaken for 150 min. The obtained findings indicate that as the adsorbent dose is raised, the efficacy of Mn removal improves. The greatest Mn removal was 96% at the optimum adsorbent dosage of BBP (0.5 g/L). More active exchangeable adsorption sites are provided by a high adsorbent dosage. Excessive adsorbent dose, on the other hand, may reduce the adsorption rate due to interference produced by adsorbent active site interaction [54]. According to Abdi et al. [55], increasing the amount of tangerine peel adsorbent enhanced Mn removal efficiency. This is because a higher dosage of adsorbent results in an increase in surface area and metal-binding sites. As a result, even though the starting metal concentration remained constant, the rate of Mn adsorption increased [50]. Furthermore, ref. [56] (2014) also reported that increasing the banana peel activated carbon (BPAC) adsorbent dosage led to higher manganese adsorption. This is because of the increased surface area and the existence of additional binding sites for manganese ions [57]. By increasing the adsorbent dose, the effective surface area for adsorption was enhanced [35].

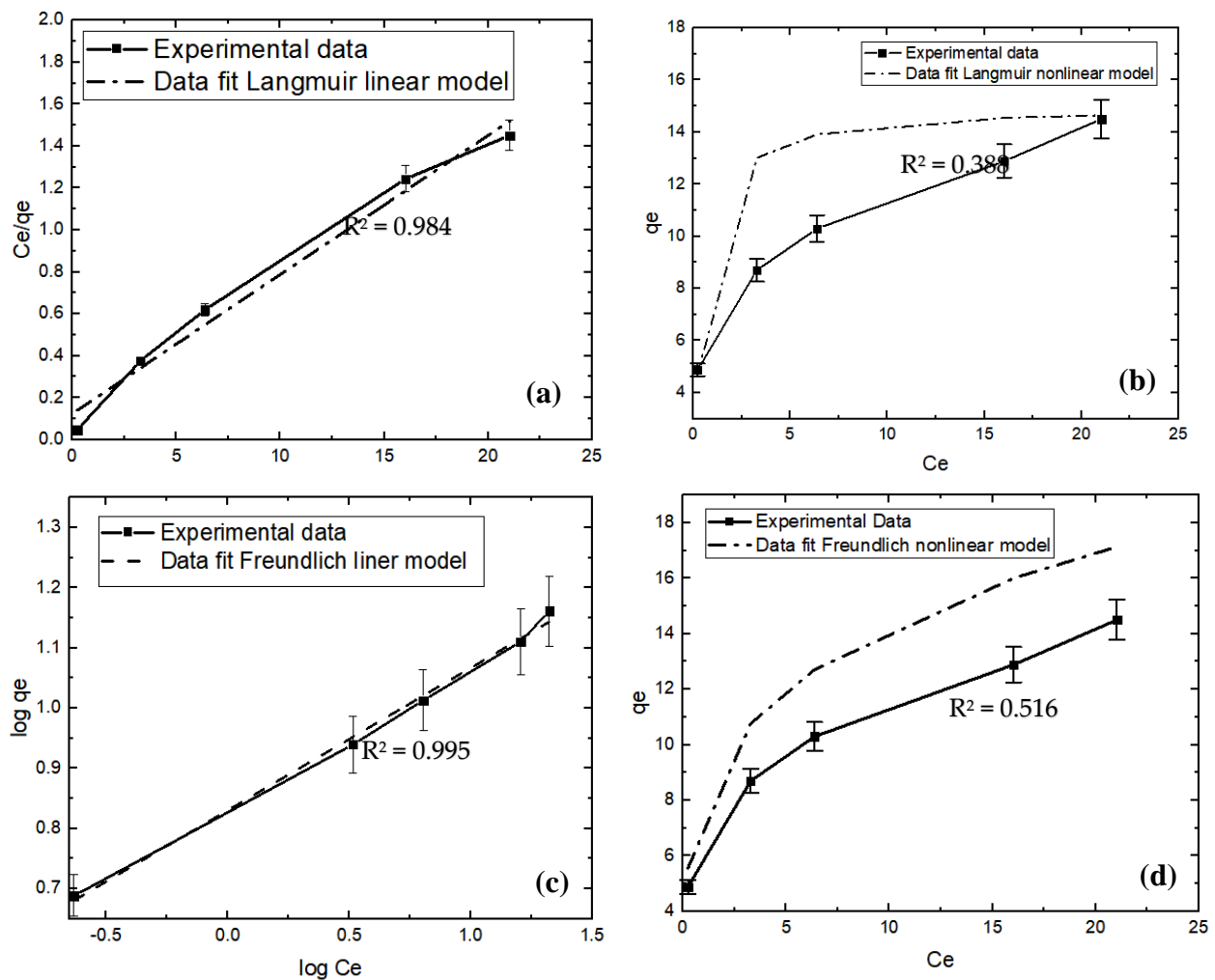


Figure 8. (a) Linear and (b) non-linear of Langmuir isotherm; (c) Linear and (d) non-linear of Freundlich isotherm model for Mn adsorption using BBP.

3.2.4. Effect of Contact Time

In 250 mL of solution, 0.5 g/L (BBP), starting Mn content of 20 mg/L, and pH of 7, the time has an important effect in the BBP adsorption, which was tested during a time span of 30–180 min. After determining the ideal pH and beginning concentration, the optimal contact time was obtained [58]. Figure 7d demonstrates that after reaching equilibrium, the optimal duration for Mn adsorption by BBP resulted in 100% removal when the contact period was prolonged up to 150 min. Marque et al. [59] found that, by utilising *Moringa oleifera* seeds as an adsorbent, they were able to remove 93% of Mn within 120 min of contact time, until equilibrium was established.

The experiment discovered that adsorption happens in two phases, the first being fast adsorption and the second being delayed release of adsorbent chemicals. This is due to the fact that the amount of adsorbed Mn has surpassed the maximum number of Mn for which the adsorbents are saturated. If a large number of adsorbents have saturated the active site on the adsorbent's surface, additional adsorption time will no longer improve adsorption and may even decrease it [58].

3.3. Comparison with Previous Studies on Mn Removal under Optimum Conditions

The result obtained under optimal Mn removal conditions for BBP in the previous experiments was performed to validate the optimal conditions. The validation experiment was conducted at 0.5 g of the BBP adsorbent dose, initial Mn concentration of 20 mg/L at pH 7, and agitated for 150 min at 125 rpm. The results were close to the previous experiment

with 98% Mn removal and clearly showed that the factors affecting the adsorption process for Mn removal were successfully determined. Table 1 shows the BBP adsorbent has remarkable adsorption capacity as compared to other studies in the literature.

Table 1. Comparison of the present study findings with previous studies.

Adsorbent	Manganese Removal (%)	pH	Contact Time (min)	Adsorbent Dosage (g)	Mn Conc. (mg/L)	Reference
Moringa seed	93	5	120	5	50	Hegazy et al. [60]
Olive pomace	91	5	120	5	50	Hegazy et al. [60]
Biochar-banana peel	46	7	180	3	10	Kim et al. [43]
Lemon peel	78.2	4	15	1	25	Meseldzija et al. [61]
Beet pulp	86.4	6	90	1	2	Ahmed et al. [57]
Tamarind fruit shell	74	3	60	1.2	100	Bangaraiah [62]
Sugarcane Bagasse	62.5	6	150	0.15	2	Ahmed et al. [57]
BBP	98	7	150	0.5	20	This study

3.4. Adsorption Isotherm Studies

Figure 8 depicts the adsorption relationships study utilising the Langmuir and Freundlich isotherms for the adsorption of Mn. The experiment was run at optimised conditions for both isotherms of Mn removal, as mentioned in the preceding section. These two models feature the most basic experiments of a wide range of operational circumstances. The Langmuir isotherm states that adsorption takes place on a homogenous surface by monolayer sorption with no interaction between the adsorbed molecules [33]. As the correlation coefficients of R^2 analysis show, the linear Langmuir and Freundlich models were best fitted according to the predicted adsorption equilibrium: 0.984 (linear Langmuir) and 0.995 (linear Freundlich), compared to non-linear Langmuir (0.388) and non-linear Freundlich (0.516), respectively.

Table 2 displayed the Langmuir and Freundlich constant isotherm on the established coefficient of R^2 from the basis of the modelling curve. The correlation coefficients of R^2 and the computed value for q_{\max} are close to the experimental q_{\max} in Figure 8a,c, indicating that the data fit the linear Langmuir model. The procedure is said to be favourable if the R_L value is between 0 and 1 ($0 < R_L < 1$) [53]. On the other hand, the determination correlation coefficients of R^2 in the linear Freundlich model were also a good fit for the experimental data, whereas the value of $1/n < 1$ indicates that the process is favourable for adsorption and the surface of the adsorbent is highly heterogeneous [53].

Table 2. Langmuir and Freundlich isotherm equilibrium parameters for manganese adsorption onto BBP adsorbent.

Model	Parameters	Non-Linear	Linear
Langmuir	q_{\max}	15 ± 1.14	15.089 ± 0.80
	R_L	2.14 ± 0.06	0.02 ± 0.12
	R^2	0.388 ± 0.07	0.984 ± 0.53
Freundlich	$1/n$	0.2365 ± 0.42	0.25 ± 0.06
	k_f	8 ± 0.12	2.294 ± 1.36
	R^2	0.516 ± 0.17	0.995 ± 0.60
Pseudo-first order	q_e	14.15 ± 1.39	62.783 ± 9.70
	K_1	1.81 ± 1.03	2.04 ± 0.70
	R^2	0.875 ± 1.51	0.840 ± 1.24
Pseudo-second order	q_e	14.33 ± 0.23	14.547 ± 2.0
	K_1	1.671 ± 1.53	0.881 ± 0.23
	R^2	0.899 ± 0.05	0.991 ± 0.01

The isotherm results obtained in the present study indicate that the experimental data for adsorption of Mn ions onto the BBP adsorbent fitted to both linear isotherm models as the values for the correlation coefficients (R^2) were both high ($R^2 > 0.98$). Mn adsorption on the BBP adsorbent can take the form of multilayers on the adsorbent's surface. However, the evidence is also compatible with linear on both isotherm models in which monolayer adsorption occurs on the BBP adsorbent, based on excellent correlation coefficients.

3.5. Adsorption Kinetics

Figure 9 depicts the linear and non-linear graphs of pseudo-first and pseudo-second-order kinetics, respectively. The regression coefficient must be high (R^2) and the calculated q_e values should be closed to the experimental q_e [59]. These criteria must be satisfied to be fitted in these kinetic models. The pseudo-second-order model accurately captured the kinetics of Mn adsorption onto the BBP adsorbent. However, the linear and non-linear pseudo-first-order models were inappropriate due to low R^2 values. The graph of pseudo-first-order in Figure 10a,c shows a poor correlation of parameters with $R^2 = 0.840$ (linear) and $R^2 = 0.875$ (non-linear), while the graph for pseudo-second-order was best described in Figure 9c with high linear regression of $R^2 = 0.991$.

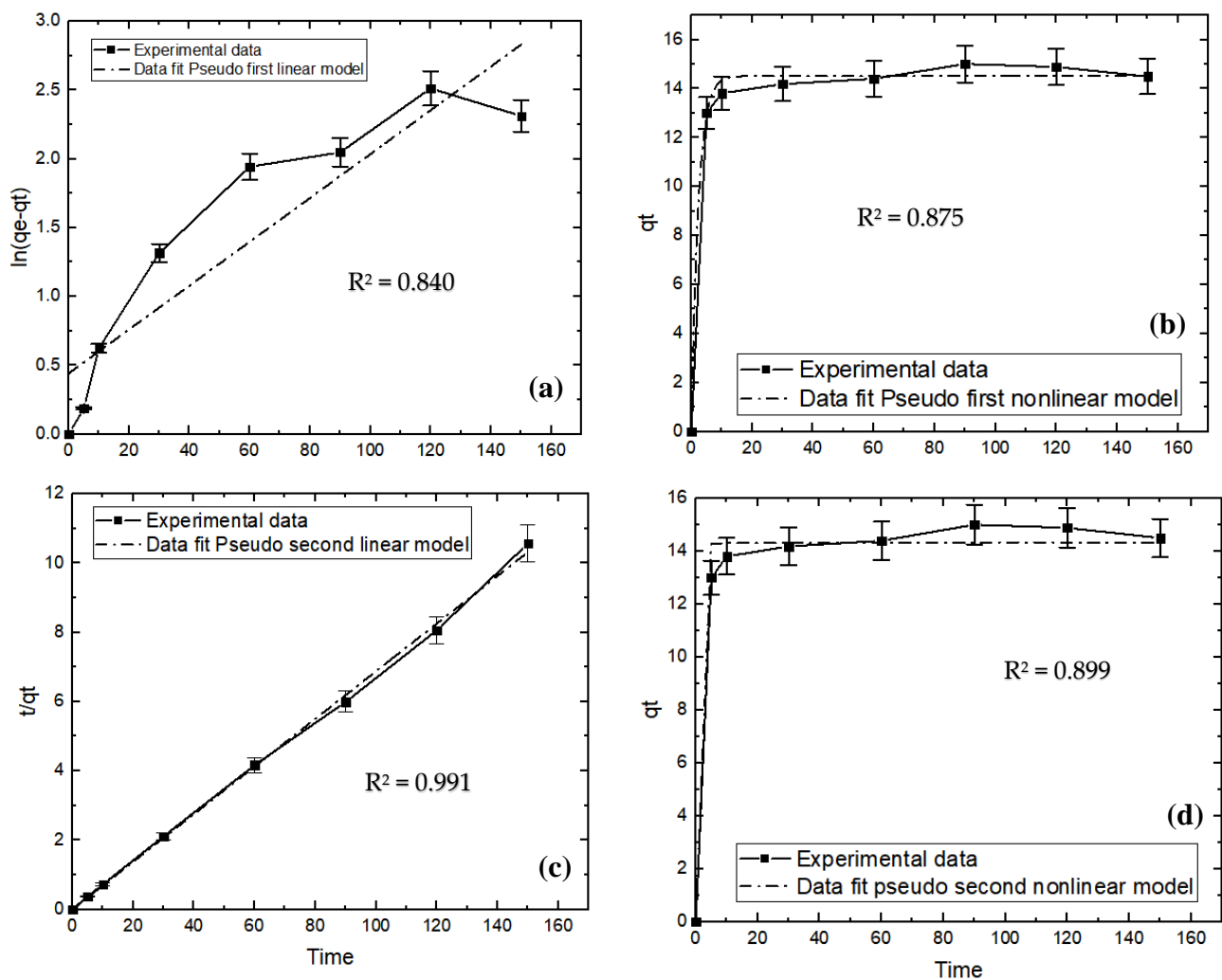


Figure 9. (a) Linear and (b) non-linear of pseudo-first-order; (c) linear and (d) non-linear of pseudo-second-order kinetic model for Mn adsorption using BBP.

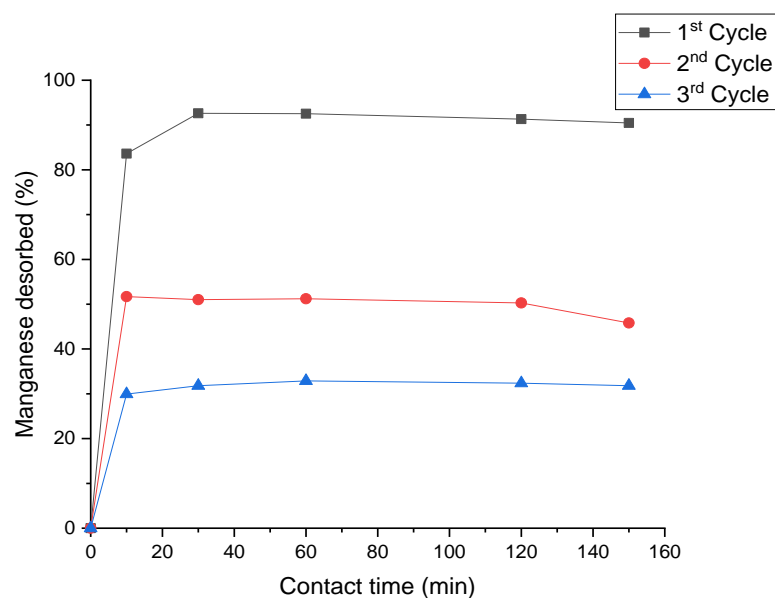


Figure 10. Desorption of manganese by BBP adsorbent.

3.6. Desorption Studies

Figure 10 shows the desorption of manganese by the BBP adsorbent. The experiment was run at the optimum condition obtained in the adsorption study, which is 0.1 M HCL acid, 0.5 g BBP adsorbent, and 150 min. A low concentration of HCL acid was used for the effective desorption process as the reaction is more stable. In the first cycle, high desorption of manganese of 92% was attained in 30 min. The recovery of the BBP adsorbent using HCL acid demonstrates a high percentage of manganese desorbed in 5 min, reaching a maximum in 30 min. However, the desorption efficiency was decreased to 51% in the second cycle and further decreased to 32% in the third cycle. The loss rate after the third cycle desorption was 60%. This might be attributed to the loss of functional groups on the BBP adsorbent surface during the regeneration process, as well as inadequate desorption. Long-term elution can cause the binding site to be destroyed or manganese ions to be left in the adsorbent [63].

Figure 11 shows the recovery of the BBP adsorbent for manganese removal. The recovery rate in the first cycle was 94.18% and decreased to 61.38% in the second cycle, followed by 40.39% in the third cycle. This showed that the adsorption recovery was effective in the first cycle but was gradually decreased in the second and third cycles. This finding shows that the BBP adsorbent has potential reusability and efficiency for reuse after the first cycle of the desorption process. As the number of desorption cycles increases, the active binding sites on the adsorbent are gradually destroyed after each cycle. As a result, the regenerated adsorbent's performance is inferior to that of the freshly manufactured adsorbent. The saturation and occupancy of adsorption sites with firmly adsorbed adsorbate can also induce a reduction in desorption efficiency [64]. Furthermore, certain chemical reagents can alter the chemical structure of adsorbents by reacting with certain of the adsorbent's components [65]. As HCL acid weakens certain active sites in the adsorbent by leaching some ions into the desorbing solution with each desorbing cycle, the adsorbent's adsorption capacity will be reduced.

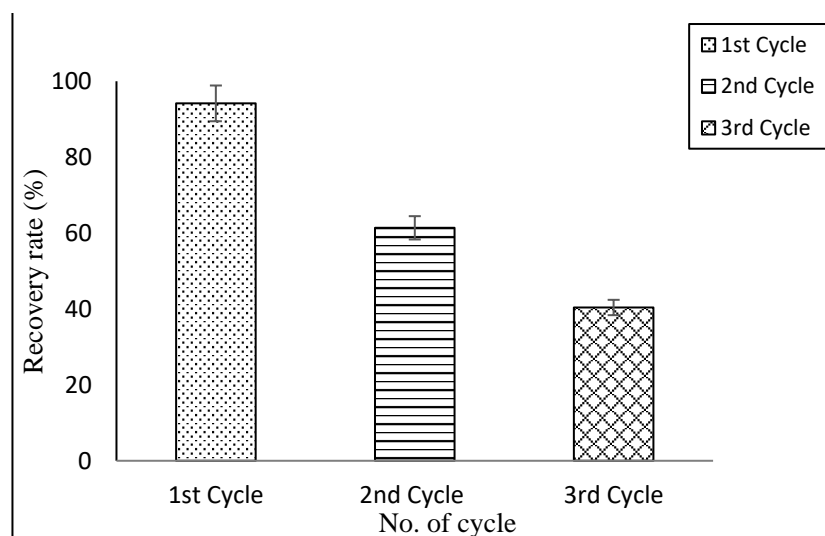


Figure 11. Recovery of BBP adsorbent for manganese removal.

4. Conclusions

The chemically modified BBP adsorbent resulted in the large surface area and crumpled shape of the adsorbent that caters to a maximum adsorption rate. The presence of hydroxyl and carboxyl groups, which play a crucial role in the adsorption process, is shown by FTIR measurement. XRD analysis suggests that the structure of BBP is amorphous, while BET analysis indicates that the size distribution of the BBP adsorbent is macropores and has the zeta potential of -9.87 to -21.1 mV. According to isotherm studies, the linear Langmuir and Freundlich model portrayed the experimental results effectively. Additionally, the linear pseudo-second-order provides a well linear regression with the R^2 of 0.99. Hence, the mechanism for the adsorption of manganese by the BBP adsorbent is by chemisorption, where the Mn ions adhere to the surface of the BBP adsorbent by a chemical bond. After the first desorption cycle, the efficiency of recycling the BBP adsorbent for additional adsorption processes is the highest, with a recovery rate of 94.18%. According to the findings, the BBP adsorbent is a potential natural adsorbent that is effective for treating water containing Mn at the optimum condition. Furthermore, the ability of the BBP adsorbent to be reused demonstrated that the adsorbent is economical and can reduce the negative impact on the environment.

Author Contributions: Conceptualization, M.S.M.; Methodology, M.S.M.; Software, N.N.R., N.M.A. and R.N.; Validation, N.M.A. and M.S.M.; Formal analysis, N.N.R. and N.M.A.; Resources, M.S.M.; Data curation, N.M.A. and S.O.; Writing—original draft, N.N.R.; Writing—review & editing, N.M.A., A.M.A., L.T.C. and R.N.; Visualization, N.M.A. and M.S.M.; Supervision, M.S.M.; Project administration, M.S.M.; Funding acquisition, M.S.M. and N.M.S. All authors have read and agreed to the published version of the manuscript.

Funding: This study was funded by the Ministry of Higher Education (MOHE), Malaysia, under the Fundamental Research Grant Scheme grant (K219) (FRGS/1/2019/TK10/UTHM/03/3). and under project grant No. M133 with the grant title “Development of Integrated Industrial Microalgae Propagation Cultivation in Pond Systems Associated with Internet of Things Pyranometer (UTHM-GIAE)”.

Informed Consent Statement: Not applicable.

Data Availability Statement: The authors confirm that the data supporting the findings of this study are available within the article. The corresponding authors affirm that this manuscript is an honest, accurate, and transparent account of the study being reported; that no important aspects of the study have been committed; and that any discrepancies from the study as planned have been explained.

Acknowledgments: The authors wish to thank the Ministry of Higher Education Malaysia for the Fundamental Research Grant Scheme grant (K219) (FRGS/1/2019/TK10/UTHM/03/3). This work was also supported and funded by project grant No. M133 “Development of Integrated Industrial Microalgae Propagation Cultivation in Pond Systems Associated with Internet of Things Pyranometer (UTHM-GIAE)”. The authors thank the parties involved in this project, especially UTHM, for providing the research facilities and equipment.

Conflicts of Interest: The authors declare no conflict of interests.

References

1. Ahmed, F.; Siwar, C.; Begum, R.A. Water resources in Malaysia: Issues and challenges. *J. Food Agric. Environ.* **2014**, *12*, 1100–1104.
2. Singh, N.B.; Nagpal, G.; Agrawal, S. Environmental Technology & Innovation Water purification by using Adsorbents: A Review. *Environ. Technol. Innov.* **2018**, *11*, 187–240.
3. Marsidi, N.; Abu Hasan, H.; Abdullah, S.R.S. A review of biological aerated filters for iron and manganese ions removal in water treatment. *J. Water Process Eng.* **2018**, *23*, 1–12. [[CrossRef](#)]
4. Zou, Y.; Wang, X.; Khan, A.; Wang, P.; Liu, Y.; Alsaedi, A.; Hayat, T.; Wang, X. Environmental Remediation and Application of Nanoscale Zero-Valent Iron and Its Composites for the Removal of Heavy Metal Ions: A Review. *Environ. Sci. Technol.* **2016**, *50*, 7290–7304. [[CrossRef](#)]
5. Milatovic, D.; Gupta, R.C. Manganese. In *Veterinary Toxicology: Basic and Clinical Principles*, 3rd ed.; Elsevier Inc.: Amsterdam, The Netherlands, 2018; pp. 445–454.
6. Tobiasson, J.E.; Bazilio, A.; Goodwill, J.; Mai, X.; Nguyen, C. Manganese Removal from Drinking Water Sources. *Curr. Pollut. Rep.* **2016**, *2*, 168–177. [[CrossRef](#)]
7. Bouchard, M.F.; Surette, C.; Cormier, P.; Foucher, D. Low level exposure to manganese from drinking water and cognition in school-age children. *Neurotoxicology* **2018**, *64*, 110–117. [[CrossRef](#)]
8. Ali, A. Removal of Mn(II) from water using chemically modified banana peels as efficient adsorbent. *Environ. Nanotechnol. Monit. Manag.* **2017**, *7*, 57–63. [[CrossRef](#)]
9. O’keeffe, L.; Pigat, S. Micronutrient exposure modelling: To build a refined safety assessment for micronutrients. *Toxicol. Lett.* **2014**, *229*, S119–S120. [[CrossRef](#)]
10. Gerke, T.L.; Little, B.J.; Maynard, J.B. Manganese deposition in drinking water distribution systems. *Sci. Total Environ.* **2016**, *541*, 184–193. [[CrossRef](#)]
11. Miah, M.R.; Ijomone, O.M.; Okoh, C.O.; Ijomone, O.K.; Akingbade, G.T.; Ke, T.; Krum, B.; da Cunha Martins, A., Jr.; Akinyemi, A.; Aranoff, N.; et al. The effects of manganese overexposure on brain health. *Neurochem. Int.* **2020**, *135*, 104688. [[CrossRef](#)]
12. Bouchard, M.F.; Sauvé, S.; Barbeau, B.; Legrand, M.; Brodeur, M.; Bouffard, T.; Limoges, E.; Bellinger, D.C.; Mergler, D. Intellectual Impairment in School-Age Children Exposed to Manganese from Drinking Water. *Environ. Health Perspect.* **2011**, *119*, 138–143. [[CrossRef](#)]
13. Ozbek, N.; Akm, S. Determination of Trace Metals in Waste Water and Their Removal Processes. In *Waste Water—Treatment Technologies and Recent Analytical Developments*; InTech: London, UK, 2013. [[CrossRef](#)]
14. Carolin, C.F.; Kumar, P.S.; Saravanan, A.; Joshiba, G.J.; Naushad, M. Efficient techniques for the removal of toxic heavy metals from aquatic environment: A review. *J. Environ. Chem. Eng.* **2017**, *5*, 2782–2799. [[CrossRef](#)]
15. Al-Jubouri, S.M.; Holmes, S.M. Hierarchically porous zeolite X composites for manganese ion-exchange and solidification: Equilibrium isotherms, kinetic and thermodynamic studies. *Chem. Eng. J.* **2017**, *308*, 476–491. [[CrossRef](#)]
16. Du, X.; Zhang, K.; Xie, B.; Zhao, J.; Cheng, X.; Kai, L.; Nie, J.; Wang, Z.; Li, G.; Liang, H. Peroxymonosulfate-assisted electro-oxidation/coagulation coupled with ceramic membrane for manganese and phosphorus removal in surface water. *Chem. Eng. J.* **2019**, *365*, 334–343. [[CrossRef](#)]
17. Alvarez-Bastida, C.; Martínez-Miranda, V.; Solache-Ríos, M.; Linares-Hernández, I.; Teutli-Sequeira, A.; Vázquez-Mejía, G. Drinking water characterization and removal of manganese. Removal of manganese from water. *J. Environ. Chem. Eng.* **2018**, *6*, 2119–2125. [[CrossRef](#)]
18. Jeirani, Z.; Sadeghi, A.; Soltan, J.; Roshani, B.; Rindall, B. Effectiveness of advanced oxidation processes for the removal of manganese and organic compounds in membrane concentrate. *Sep. Purif. Technol.* **2015**, *149*, 110–115. [[CrossRef](#)]
19. Seyedpour, S.F.; Rahimpour, A.; Mohsenian, H.; Taherzadeh, M.J. Low fouling ultrathin nanocomposite membranes for efficient removal of manganese. *J. Membr. Sci.* **2018**, *549*, 205–216. [[CrossRef](#)]
20. Ihsanullah; Abbas, A.; Al-Amer, A.M.; Laoui, T.; Al-Marri, M.J.; Nasser, M.S.; Khraisheh, M.; Atieh, M.A. Heavy metal removal from aqueous solution by advanced carbon nanotubes: Critical review of adsorption applications. *Sep. Purif. Technol.* **2016**, *157*, 141–161. [[CrossRef](#)]
21. Ahmadi, S.; Ganjidoust, H. Using banana peel waste to synthesize BPAC/ZnO nanocomposite for photocatalytic degradation of Acid Blue 25: Influential parameters, mineralization, biodegradability studies. *J. Environ. Chem. Eng.* **2021**, *9*, 106010. [[CrossRef](#)]
22. Jawed, A.; Pandey, L.M. Application of bimetallic Al-doped ZnO nano-assembly for heavy metal removal and decontamination of wastewater. *Water Sci. Technol.* **2019**, *80*, 2067–2078. [[CrossRef](#)]

23. Burakov, A.E.; Galunin, E.V.; Burakova, I.V.; Kucherova, A.E.; Agarwal, S.; Tkachev, A.G.; Gupta, V.K. Adsorption of heavy metals on conventional and nanostructured materials for wastewater treatment purposes: A review. *Ecotoxicol. Environ. Saf.* **2018**, *148*, 702–712. [[CrossRef](#)]
24. Shahraki, H.S.; Bushra, R.; Shakeel, N.; Ahmad, A.; Quratulen; Ahmad, M.; Ritzoulis, C. Papaya peel waste carbon dots/reduced graphene oxide nanocomposite: From photocatalytic decomposition of methylene blue to antimicrobial activity. *J. Bioresour. Bioprod.* **2023**, *8*, 162–175. [[CrossRef](#)]
25. Liu, L.; Tan, S.; Horikawa, T.; Do, D.; Nicholson, D.; Liu, J. Water adsorption on carbon—A review. *Adv. Colloid Interface Sci.* **2017**, *250*, 64–78. [[CrossRef](#)]
26. Sajid, M.; Nazal, M.K.; Ihsanullah; Baig, N.; Osman, A.M. Removal of heavy metals and organic pollutants from water using dendritic polymers based adsorbents: A critical review. *Sep. Purif. Technol.* **2018**, *191*, 400–423. [[CrossRef](#)]
27. Obey, G.; Adelaide, M.; Ramaraj, R. Biochar derived from non-customized matamba fruit shell as an adsorbent for wastewater treatment. *J. Bioresour. Bioprod.* **2022**, *7*, 109–115. [[CrossRef](#)]
28. Jjagwe, J.; Olupot, P.W.; Menya, E.; Kalibbala, H.M. Synthesis and Application of Granular Activated Carbon from Biomass Waste Materials for Water Treatment: A Review. *J. Bioresour. Bioprod.* **2021**, *6*, 292–322. [[CrossRef](#)]
29. Herawati, D.; Santoso, S.D.; Amalina, I. Kondisi Optimum Adsorpsi-Fluidisasi Zat Warna Limbah Tekstil Menggunakan Adsorben Jantung Pisang. *J. Sain Health* **2018**, *2*, 1–7. [[CrossRef](#)]
30. Wu, L.; Zhang, G.; Lin, J. The Physicochemical Properties and Adsorption Characteristics of Processed Pomelo Peel as a Carrier for Epigallocatechin-3-Gallate. *Molecules* **2020**, *25*, 4249. [[CrossRef](#)]
31. Surovka, D.; Pertile, E. Sorption of Iron, Manganese, and Copper from Aqueous Solution Using Orange Peel: Optimization, Isothermic, Kinetic, and Thermodynamic Studies. *Pol. J. Environ. Stud.* **2017**, *26*, 795–800. [[CrossRef](#)]
32. Zavala-Franco, A.; Hernández-Patlán, D.; Solís-Cruz, B.; López-Arellano, R.; Tellez-Isaias, G.; Vázquez-Durán, A.; Méndez-Albores, A. Assessing the Aflatoxin B1 Adsorption Capacity between Biosorbents Using an In Vitro Multicompartmental Model Simulating the Dynamic Conditions in the Gastrointestinal Tract of Poultry. *Toxins* **2018**, *10*, 484. [[CrossRef](#)]
33. Volkov, D.S.; Rogova, O.B.; Proskurnin, M.A. Temperature dependences of IR spectra of humic substances of brown coal. *Agronomy* **2021**, *11*, 1822. [[CrossRef](#)]
34. Yang, C.; Wu, H.; Cai, M.; Li, Y.; Guo, C.; Han, Y.; Zhang, Y.; Song, B. Valorization of food waste digestate to ash and biochar composites for high performance adsorption of methylene blue. *J. Clean. Prod.* **2023**, *397*, 136612. [[CrossRef](#)]
35. Adekola, F.A.; Hodonou, D.S.S.; Adegoke, H.I. Thermodynamic and kinetic studies of biosorption of iron and manganese from aqueous medium using rice husk ash. *Appl. Water Sci.* **2016**, *6*, 319–330. [[CrossRef](#)]
36. Fathi, A.; Gahlan, A.A.; Farghaly, O.A. Decontamination of Copper and Manganese from Aqueous Media by Untreated and Chemically Treated Sugarcane Bagasse: A Comparative Study. *Chem. Adv. Mater.* **2020**, *5*, 15–33.
37. Samimi, S.; Maghsoudnia, N.; Eftekhari, R.B.; Dorkoosh, F. Lipid-Based Nanoparticles for Drug Delivery Systems. In *Characterization and Biology of Nanomaterials for Drug Delivery*; Elsevier: Amsterdam, The Netherlands, 2019; pp. 47–76. [[CrossRef](#)]
38. Abdeen, Z.; Mohammad, S.; Mahmoud, M. Adsorption of Mn (II) ion on polyvinyl alcohol/chitosan dry blending from aqueous solution. *Environ. Nanotechnol. Monit. Manag.* **2015**, *3*, 1–9. [[CrossRef](#)]
39. Bediako, J.K.; Sarkar, A.K.; Lin, S.; Zhao, Y.; Song, M.-H.; Choi, J.-W.; Cho, C.-W.; Yun, Y.-S. Characterization of the residual biochemical components of sequentially extracted banana peel biomasses and their environmental remediation applications. *Waste Manag.* **2019**, *89*, 141–153. [[CrossRef](#)]
40. Chen, L.; Fang, Y.; Jin, Y.; Chen, Q.; Zhao, Y.; Xiao, Y.; Zhao, H. Biosorption of Cd²⁺ by untreated dried powder of duckweed *Lemna aequinoctialis*. *Desalination Water Treat.* **2013**, *53*, 183–194. [[CrossRef](#)]
41. DeRosa, T.F. *Advances in Synthetic Organic Chemistry and Methods Reported in US Patents*; Elsevier: Amsterdam, The Netherlands, 2006.
42. Mohamed, R.M.; Hashim, N.; Abdullah, S.; Abdullah, N.; Mohamed, A.; Daud, M.A.A.; Muzakkar, K.F.A. Adsorption of Heavy Metals on Banana Peel Bioadsorbent. *J. Phys. Conf. Ser.* **2020**, *1532*, 012014. [[CrossRef](#)]
43. Kim, H.; Ko, R.-A.; Lee, S.; Chon, K. Removal Efficiencies of Manganese and Iron Using Pristine and Phosphoric Acid Pre-Treated Biochars Made from Banana Peels. *Water* **2020**, *12*, 1173. [[CrossRef](#)]
44. Mahmoodi, N.M.; Taghizadeh, M.; Taghizadeh, A. Mesoporous activated carbons of low-cost agricultural bio-wastes with high adsorption capacity: Preparation and artificial neural network modeling of dye removal from single and multicomponent (binary and ternary) systems. *J. Mol. Liq.* **2018**, *269*, 217–228. [[CrossRef](#)]
45. Goher, M.E.; Hassan, A.M.; Abdel-Moniem, I.A.; Fahmy, A.H.; Abdo, M.H.; El-Sayed, S.M. Removal of aluminum, iron and manganese ions from industrial wastes using granular activated carbon and Amberlite IR-120H. *Egypt. J. Aquat. Res.* **2015**, *41*, 155–164. [[CrossRef](#)]
46. Maia, L.S.; Duizit, L.D.; Pinhatio, F.R.; Mulinari, D.R. Valuation of banana peel waste for producing activated carbon via NaOH and pyrolysis for methylene blue removal. *Carbon Lett.* **2021**, *31*, 749–762. [[CrossRef](#)]
47. García-Mendieta, A.; Olguín, M.T.; Solache-Ríos, M. Biosorption properties of green tomato husk (*Physalis philadelphica* Lam) for iron, manganese and iron–manganese from aqueous systems. *Desalination* **2012**, *284*, 167–174. [[CrossRef](#)]
48. Mumtaz, M.W.; Mukhtar, H.; Anwar, F.; Saari, N. RSM Based Optimization of Chemical and Enzymatic Transesterification of Palm Oil: Biodiesel Production and Assessment of Exhaust Emission Levels. *Sci. World J.* **2014**, *2014*, 526105. [[CrossRef](#)]
49. Akl, M.A.; Yousef, A.M.; AbdElnasser, S. Removal of Iron and Manganese in Water Samples Using Activated Carbon Derived from Local Agro-Residues. *J. Chem. Eng. Process Technol.* **2013**, *4*. [[CrossRef](#)]

50. Esfandiar, N.; Nasernejad, B.; Ebadi, T. Removal of Mn(II) from groundwater by sugarcane bagasse and activated carbon (a comparative study): Application of response surface methodology (RSM). *J. Ind. Eng. Chem.* **2014**, *20*, 3726–3736. [[CrossRef](#)]
51. Feizi, M.; Jalali, M. Removal of heavy metals from aqueous solutions using sunflower, potato, canola and walnut shell residues. *J. Taiwan Inst. Chem. Eng.* **2015**, *54*, 125–136. [[CrossRef](#)]
52. Idrees, M.; Batool, S.; Ullah, H.; Hussain, Q.; Al-Wabel, M.I.; Ahmad, M.; Hussain, A.; Riaz, M.; Ok, Y.S.; Kong, J. Adsorption and thermodynamic mechanisms of manganese removal from aqueous media by biowaste-derived biochars. *J. Mol. Liq.* **2018**, *266*, 373–380. [[CrossRef](#)]
53. Adeogun, A.I.; Idowu, M.A.; Ofudje, A.E.; Kareem, S.O.; Ahmed, S.A. Comparative biosorption of Mn(II) and Pb(II) ions on raw and oxalic acid modified maize husk: Kinetic, thermodynamic and isothermal studies. *Appl. Water Sci.* **2013**, *3*, 167–179. [[CrossRef](#)]
54. Iftekhar, S.; Ramasamy, D.L.; Srivastava, V.; Asif, M.B.; Sillanpää, M. Understanding the factors affecting the adsorption of Lanthanum using different adsorbents: A critical review. *Chemosphere* **2018**, *204*, 413–430. [[CrossRef](#)]
55. Abdić, M.; Memić, M.; Šabanović, E.; Sulejmanović, J.; Begić, S. Adsorptive removal of eight heavy metals from aqueous solution by unmodified and modified agricultural waste: Tangerine peel. *Int. J. Environ. Sci. Technol.* **2018**, *15*, 2511–2518. [[CrossRef](#)]
56. Mahmoud, M.S.; Ahmed, S.M.; Mohammad, S.G.; Elmagd, A.M.A. Evaluation of Egyptian Banana Peel (*Musa* sp.) as a Green Sorbent for Groundwater Treatment. *Int. J. Eng. Technol.* **2014**, *4*, 648–659.
57. Ahmed, S.A.; El-Roudi, A.M.; Salem, A.A. Removal of Mn(II) from Ground Water by Solid Wastes of Sugar Industry. *J. Environ. Sci. Technol.* **2015**, *8*, 338–351. [[CrossRef](#)]
58. Kurniawati, D.; Bahrizal; Sari, T.K.; Adella, F.; Sy, S. Effect of Contact Time Adsorption of Rhodamine B, Methyl Orange and Methylene Blue Colours on Langsat Shell with Batch Methods. *J. Phys. Conf. Ser.* **2021**, *1788*, 012008. [[CrossRef](#)]
59. Marques, T.L.; Alves, V.N.; Coelho, L.M.; Coelho, N.M.M. Assessment of the Use of Moringa oleifera Seeds for Removal of Manganese Ions from Aqueous Systems. *Bioresources* **2013**, *8*, 2738–2751. [[CrossRef](#)]
60. Hegazy, I.; Ali, M.E.A.; Zaghlool, E.H.; Elsheikh, R. Heavy metals adsorption from contaminated water using moringa seeds/olive pomace byproducts. *Appl. Water Sci.* **2021**, *11*, 95. [[CrossRef](#)]
61. Meseldžija, S.; Petrović, J.; Onjia, A.E.; Volkov-Husović, T.; Nešić, A.; Vukelić, N. Removal of Fe²⁺, Zn²⁺ and Mn²⁺ from the mining wastewater by lemon peel waste. *J. Serb. Chem. Soc.* **2020**, *85*, 1371–1382. [[CrossRef](#)]
62. Bangaraiah, P. Biosorption of Manganese using Tamarind fruit Shell Powder as a Biosorbent. *Res. J. Pharm. Technol.* **2018**, *11*, 4313–4316. [[CrossRef](#)]
63. Li, X.; Yu, X.; Liu, L.; Yang, J.; Liu, S.; Zhang, T. Preparation, characterization serpentine-loaded hydroxyapatite and its simultaneous removal performance for fluoride, iron and manganese. *RSC Adv.* **2021**, *11*, 16201–16215. [[CrossRef](#)]
64. Vakili, M.; Deng, S.; Cagnetta, G.; Wang, W.; Meng, P.; Liu, D.; Yu, G. Regeneration of chitosan-based adsorbents used in heavy metal adsorption: A review. *Sep. Purif. Technol.* **2019**, *224*, 373–387. [[CrossRef](#)]
65. Omorogie, M.O.; Babalola, J.O.; Unuabonah, E.I. Regeneration strategies for spent solid matrices used in adsorption of organic pollutants from surface water: A critical review. *Desalination Water Treat.* **2014**, *57*, 518–544. [[CrossRef](#)]

Disclaimer/Publisher's Note: The statements, opinions and data contained in all publications are solely those of the individual author(s) and contributor(s) and not of MDPI and/or the editor(s). MDPI and/or the editor(s) disclaim responsibility for any injury to people or property resulting from any ideas, methods, instructions or products referred to in the content.